Arabian Journal for Science and Engineering (2022) 47:7105–7122
https://doi.org/10.1007/s13369-021-06521-7

RESEARCH ARTICLE-CHEMISTRY

Synthesis, Spectroscopic and Biological Investigation of a New Ca(II) Complex of Meloxicam as Potential COX-2 Inhibitor

Malka M. Samra[1] · Aatika Sadia[1] · Muhammad Azam[1] · Muhammad Imran[1] · Irfan Ahmad[2,3] · Muhammad Asim Raza Basra[1]

Received: 26 February 2021 / Accepted: 16 December 2022 / Published online: 19 January 2022

Abstract
Drug development on basis of coordination compounds provides versatile structural and functional properties as compared to other organic compounds. In the present study, a new Ca(II) complex of meloxicam was synthesized and characterized by elemental analysis, FT-IR, UV–Vis, ^{13}C NMR, SEM–EDX, powder XRD and thermal analysis (TGA). The Ca(II) complex was investigated for its in vitro, in vivo biological activities and in silico docking analysis against COX-1 and COX-2. The spectral analysis indicates that the meloxicam acts as a deprotonated bidentate ligand (coordinated to the metal atom through the amide oxygen and the nitrogen atom of the thiazolyl ring) in the complex. SEM–EDX and powder XRD analysis depicted crystalline morphology of Ca(II) complex with a crystalline size of 32.86 nm. The in vitro biological activities were evaluated by five different antioxidant methods and COX inhibition assay, while in vivo activities were evaluated by carrageenan-, histamine- and PGE_2-induced paw edema methods and acetic acid-induced writhing test. The Ca(II) complex showed prominent antioxidant activities and was found to be more selective toward COX-2 (43.77) than COX-1 as compared to meloxicam. It exhibited lower toxicity (LD_{50} 1000 mg/Kg) and significantly inhibited carrageenan- and PGE_2-induced inflammation at 10 mg/Kg ($P < 0.05$), but no significant effect was observed on histamine-induced inflammation. Moreover, Ca(II) complex significantly reduced the number of writhes induced by acetic acid ($P < 0.05$). The in silico molecular docking data revealed that Ca(II) complex obstructed COX-2 (dock score 6438) more effectively than COX-1 (dock score 5732) as compared to meloxicam alone.

Keywords Meloxicam · Calcium · Antioxidant · Inflammation · Molecular docking

1 Introduction

In the recent times, the inflammatory diseases such as autoimmune and infectious diseases have exponentially escalated. The management of never-endingly transmitted infectious diseases and various microbial and viral infections like multisystem inflammatory syndrome and Coronavirus Disease 2019 (COVID-19) requires effective anti-inflammatory and analgesic drugs to cure the post-infection inflammatory events [1, 2]. Likewise, the severe and prevalent autoimmune diseases such as allergic asthma and rheumatoid arthritis manifest chronic and acute inflammation characterized by pain, edema and redness and are usually treated by non-steroidal anti-inflammatory drugs (NSAIDs), glucocorticoids and disease-modifying antirheumatic drugs (DMARDs) [3–5]. The NSAIDs are widely prescribed and also used over the counter for alleviating the conditions of the different diseases by inhibiting the prostaglandin endoperoxide synthase enzyme also called cyclooxygenase (COX) [6]. Among the isoforms of enzyme, designated as COX-1 and COX-2, COX-1 plays housekeeping actions and is responsible for maintaining the protective lining of the gastrointestinal tract (GIT), while COX-2 is responsible for the synthesis and migration of pro-inflammatory cytokines to the site of inflammation [7, 8].

✉ Muhammad Asim Raza Basra
asimarbasra@gmail.com; asimbasra.chem@pu.edu.pk

[1] School of Chemistry, University of The Punjab, New Campus, Lahore, Pakistan

[2] Research Center for Advanced Materials Science (RCAMS), King Khalid University, P.O. Box 9004, Abha 61413, Saudi Arabia

[3] Department of Chemistry, College of Science, King Khalid University, P.O. Box 9004, Abha 61413, Saudi Arabia

The NSAIDs are designed to suppress inflammation by obstructing the enzyme COX-2 through receptor analogy, thus preventing the synthesis and accumulation of pro-inflammatory cytokines and macrophages at the site of inflammation [9]. Free radicals triggered by neutrophils and macrophages play a key role in inflammatory reactions as they enhance the inflammatory response by increasing the production of cytokines and chemokines (in the positive feedback mechanism) and also damage local cells through oxidation and nitration [10, 11]. Reactive oxygen species (ROS) production typically increased during inflammatory process, and it was shown that some of the NSAIDs have potential to interact with reactive species and therefore preventing oxidative damage [12].

Meloxicam (4-hydroxy-2-methyl-*N*-(5-methyl-1,3-thiazol-2-yl)-1,1-dioxo-1λ^6,2-benzothiazine-3-carboxamide, $C_{14}H_{13}N_3O_4S_2$, Fig. 1) is NSAID of oxicam family, often used in inflammatory diseases such as rheumatoid arthritis or osteoarthritis [13]. It is designed to selectively inhibit the COX-2; however, the presence of acidic groups in its structure still hinders the proper management of inflammation [14]. Other than its anti-inflammatory and analgesic properties, meloxicam has been reported to reduce the formation of singlet oxygen and other reactive oxidants [15]. Given that inflammation has a complex pathogenesis, complexation of meloxicam with suitable metal ion may increase its anti-radical effectiveness and efficiency of anti-inflammatory treatment. Till date numerous metal complexes of meloxicam have been synthesized to alleviate the inflammation as well as oxidative stress without causing harm to the body. Metal ions perform remarkable roles in biological regulations [16], and the existence of the metallic ions can also affect the bioavailability of drugs [17]. Metal complexes have a greater impact on the target tissues as compared to the sole drugs due to their synergic action [18]. However, most of the reported metal complexes have greater toxicity plausibly due to the poisonous nature of the metals used [19]. Therefore, bio-metals are considered more desirable for preparing such drugs as these metals would not pose toxicity in the body [20].

The present work was designed to synthesize and characterize a new calcium complex of meloxicam through different spectroscopic techniques. The Ca(II) complex was assessed for in vitro antioxidant and COX inhibition assays, in vivo anti-inflammatory activities through carrageenan-, histamine- and prostaglandin E2-induced edema, while analgesic efficacy was evaluated by acetic acid-induced writhings. Inhibitory effect on COX-2 was investigated by in silico molecular docking for visualizing the in vivo anti-inflammatory and analgesic efficiency of new Ca(II) complex of meloxicam.

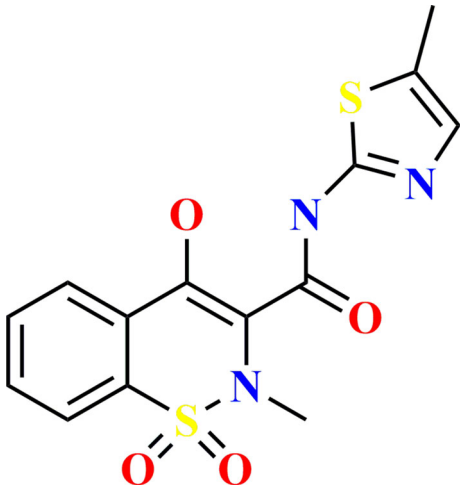

Fig. 1 Molecular structure of meloxicam

2 Material and Methods

2.1 Material

All chemicals used were of analytical reagent grade and of the highest purity available. Meloxicam was obtained from Alcon biosciences private limited (India). $CaCl_2$ anhydrous, NaOH, DPPH (2,2-diphenyl-1-picrylhydrazyl), ABTS (2,2'-azino-bis(3-ethylbenzothiazoline-6-sulphonic acid)), potassium persulfate, $FeCl_3$ anhydrous, 1,10-phenanthroline 1-hydrate, potassium ferricyanide, ammonium molybdate, anhydrous monosodium phosphate, carrageenan, histamine, prostaglandin E2 (PGE_2), sodium carboxymethyl cellulose (Na-CMC) and DMSO were purchased from Sigma-Aldrich. Sulfuric acid and trichloroacetic acid (TCA) were obtained from Acros organics and spectrum chemicals, respectively. Analytical grade ethanol and methanol were used.

2.2 Synthesis of Ca(II) Complex of Meloxicam

The new calcium metal complex of meloxicam was synthesized by following previously reported protocol with few modifications [21]. Briefly, 0.5 mM ethanolic solution of anhydrous $CaCl_2$ was treated with 1 mM ethanolic solution of meloxicam at pH 7. The mixture was stirred overnight and was then placed in water bath at 60 °C until precipitates were condensed. The precipitates were filtered, washed with hot ethanol and then dried at ambient temperature. The overnight stirring was done to obtain good yield of calcium metal complex which is difficult to achieve due to inert nature of calcium metal as compared to reactive metals we reported in our previous work [22].

2.2.1 [Ca(4-hydroxy-2-methyl-N-(5-methyl-1,3-thiazol-2-yl)-1,1-dioxo-1λ6,2-benzothiazine-3-carboxamide)$_2$(H_2O)$_2$]

Molecular formula; $C_{28}H_{28}N_6O_{10}S_4Ca$, Pale white, Yield: 86%, M.P.: decomposed above 300 °C. Molecular weight: 776.04 g/mole, IR (KBr, cm^{-1}): 1605 $(C{=}O)_{amide}$, 1069 $(SO_2)_{asym}$ and 1046 $(SO_2)_{sym}$. UV (DMSO) λ_{max} (cm^{-1}): 375, 280 nm. Anal. for $C_{28}H_{28}N_6O_{10}S_4Ca$, Calcd: C, 43.29; H, 3.63; N, 10.82; S, 16.47% Found: C, 36.60; H, 3.28; N, 8.73; S, 14.30%.

2.3 Characterization

The UV–visible spectroscopy was performed on T90 + UV/VIS spectrometer PG instrument within the range of 200–450 nm using DMSO as blank. Melting and decomposition temperatures were measured on Gallen Kamp melting point apparatus. FTIR of the dry sample was performed using PerkinElmer Spectrum-100 (KBr crystal). Elemental analysis was performed using a Euro EA elemental analyzer, and ^{13}C NMR spectra were recorded by Bruker Avance 400. Metal contents were obtained through atomic absorption spectrometry and flame photometry performed by PerkinElmer AA Analyst-100 and Sherwood 410 flame photometer, respectively. Field emission scanning electron microscopy with energy-dispersive spectroscopy analysis (FESEM-EDS) of the sample was done by Nova Nano SEM 450 field emission scanning electron microscope (FESEM). Powder X-ray diffraction (XRD) was carried out with Cu K_α between $2\theta^\circ = 5$–50° with a step size of 0.04° using Bruker D8 Discover XRD system. The thermogravimetric analysis (TGA) was performed by SDT Q600 thermogravimetric analyzer to determine the thermal stability of the metal complex. The sample (0.05 g) was subjected to temperature rise from 25 to 1000 °**C** in the presence of N_2 environment, and the rate of temperature rise was kept 10 °**C** per minute. Temperature T_{max} (°C) at each step of degradation was recorded. Coats Redfern equation was used to determine the energy of activation based on the results of TGA [23].

2.4 Biological Evaluation

2.4.1 In Vitro Antioxidant Assays

DPPH Free Radical Scavenging Assay The DPPH assay was performed to evaluate the radical scavenging activity of synthesized calcium complex. The stock solution of the complex was prepared in DMSO which was serially diluted to test concentrations from 2000 to 1.95 μM with ethanol, respectively. The ethanolic solution of DPPH was treated with test concentrations of each sample and incubated at 37 °C. The absorbance was recorded at 517 nm after 15, 30, 45, 60 and 120 min of incubation against ethanol used as blank. Ascorbic acid was used as standard, and IC_{50} of the synthesized metal complex was calculated with following equation [24].

$$\%\ \text{DPPH scavenging activity} = \left(\text{Abs (control)} - \text{Abs}\left(\text{sample}\right)/\text{Abs (control)}\right) \times 100$$

ABTS$^{\bullet+}$ Assay ABTS activity was conducted to determine radical scavenging ability of the synthesized Ca(II) complex. $ABTS^{\bullet+}$reagent was prepared by mixing equal volumes of aqueous 7 mM ABTS and 2.45 mM potassium persulfate. The resulting mixture was incubated for 12–16 h in dark at ambient temperature followed by dilution with ethanol till the absorbance reached to 0.7 ± 0.02 at 734 nm. The stock solution of the complex in DMSO was serially diluted to test concentrations from 2000 to 1.95 μM with ethanol, respectively. The $ABTS^{\bullet+}$ reagent was treated with test concentrations of each sample and incubated in dark at ambient temperature. The absorbance of samples was recorded at 734 nm after the intervals of 5, 15, 30, 45, 60 and 120 min of incubation against ethanol used as blank. Ascorbic acid was used as standard, and the IC_{50} of the synthesized metal complex was calculated with following equation [24].

$$\%\ \text{ABTS scavenging activity} = \left(\text{Abs (control)} - \text{Abs}\left(\text{sample}\right)/\text{Abs (control)}\right) \times 100$$

Iron Chelating Assay The iron chelating activity was performed to assess the reducing ability of the synthesized Ca(II) complex. The stock solution of the complex prepared in DMSO was serially diluted to test concentrations from 2000 to 1.95 μM with methanol, respectively. The sample solution was mixed with 0.05% methanolic *o*-phenanthroline solution followed by 200 μM freshly prepared methanolic $FeCl_3$ solution. The absorbance of samples was recorded at 512 nm after 10, 30, 45, 60 and 120 min against methanol used as blank. Ascorbic acid was used as standard, and IC_{50} of the synthesized metal complex was calculated with following equation [24].

$$\%\ \text{Fe chelating activity} = \left(\text{Abs}\left(\text{sample}\right) - \text{Abs (control)}/\text{Abs}\left(\text{sample}\right)\right) \times 100$$

$FeCl_3$ Reducing Power The $FeCl_3$ reducing power activity of the synthesized Ca(II) complex was determined by following established protocol. The stock solution of the complex was serially diluted to test concentrations from 2000 to 1.95 μM with ethanol, respectively. The sample solution was treated with 1% potassium ferricyanide solution followed by incubation at 50 °C for 20 min. The samples were then allowed to cool at room temperature, and 2.5 mL TCA was added to stop the reaction, which is followed by centrifugation at 3000 RPM for 10 min. The supernatant was diluted with water and treated with 0.1% freshly prepared $FeCl_3$ solution. The

absorbance of samples was recorded at 700 nm after 10, 30, 45, 60 and 120 min against ethanol used as blank. Ascorbic acid was used as standard, and the IC_{50} of the synthesized metal complex was calculated with following equation [24].

$$\%\ \text{Fe reducing activity} = \left(\text{Abs}\left(\text{sample}\right)/\text{Abs}\left(\text{control}\right) - 1\right) \times 100$$

Phospho-Molybdenum Assay The phospho-molybdenum (PM) activity was performed to assess the reducing ability of the synthesized Ca(II) complex. The PM reagent was prepared by mixing equal volumes of 0.6 M H_2SO_4 (0.6 M), aqueous ammonium molybdate solution (4 mM) and aqueous sodium phosphate solution (28 mM). Stock solution of the complex was prepared in DMSO which was serially diluted to test concentrations from 2000 to 1.95 μM with ethanol, respectively. The sample solution was treated with PM reagent followed by incubation at 95 °C for 90 min. The absorbance of samples was recorded at 765 nm after 15, 30, 45 and 60 min against ethanol used as blank. Ascorbic acid was used as standard, and the IC_{50} of the synthesized metal complex was calculated with following equation [24].

$$\%\ \text{Mo reducing power} = \left(\text{Abs}\left(\text{sample}\right)/\text{Abs}\left(\text{control}\right) - 1\right) \times 100$$

2.4.2 In Vitro Cyclooxygenase Inhibition Assay

The COX inhibitor Screening Assay Kit (Catalog No. 560131, Cayman Chemical, Ann Arbor, MI, USA) was used to measure the cyclooxygenase inhibitory potential of synthesized Ca(II) meloxicam complex. The ovine COX-1 and human recombinant COX-2 activity directly measure $PGF_{2\alpha}$ produced by $SnCl_2$ reduction of COX-derived PGH_2. The prostanoid product is quantified via enzyme immunoassay (EIA) using a broadly specific antibody that binds to all the major prostaglandin compounds. Briefly, control value was obtained in the absence of compound. The COX enzyme was mixed with different concentration of tested compound and heme and incubated for 10 min at 37 °C. The reaction was initiated by adding arachidonic acid, and all tubes were incubated for another 2 min at 37 °C. The efficacy of compound was determined as the concentration causing 50% enzyme inhibition (IC_{50}). The selectivity index (SI values) was calculated as IC_{50} (COX-1)/IC_{50} (COX-2) [25, 26].

2.4.3 In Vivo Assays

Animals All in vivo experimentation of the synthesized Ca(II) complex of meloxicam was performed using Sprague–Dawley (SD) rats, 10–12 weeks old (150–200 g), maintained at controlled temperature (25 ± 5 °C) and humidity (50 ± 10%) in the institutional animal house. The animals were exposed to 12 h light and dark cycle and had free access to autoclaved tap water and pathogen-free feed for 24 h. International ethical guidelines were followed for the care of laboratory animals to provide them with a healthy and clean environment. Experiments were approved by Institutional Ethical Committee, University of the Punjab, Lahore (Approval No. D/025/2018, March 07, 2018).

Acute Toxicity of Ca(II) Complex of Meloxicam Acute toxicity of the Ca(II) complex was tested, and safe dose was calculated as per organization for economic cooperation and development (OECD) test guideline 425 [27]. Rats were randomly divided into eight groups of either sex ($n = 5$) and were treated with 5, 25, 50, 100, 250, 500, 1000 and 2000 mg/Kg dose of Ca(II) complex orally. The control group received CMC (0.5%) at a dose 10 mL/kg. All the animals were observed randomly for any signs of toxicity during first 4 h, and then, the numbers of dead animals were counted after 24 h. LD_{50} was calculated by the previously used method [28, 29].

In Vivo *Anti-Inflammatory Activity* Carrageenan-induced paw edema method was followed to evaluate the anti-inflammatory effect of meloxicam and its Ca(II) complex [30]. The rats were randomly divided into five groups ($n = 6$): the Carrageenan group, low (5 mg/Kg), medium (10 mg/Kg) and high (20 mg/Kg) dose Ca(II) complex groups and standard meloxicam (10 mg/Kg) group [31]. Rats in the carrageenan control group received oral gavage of 0.5% CMC and served as control group, while rats in standard meloxicam and low, medium and high dose Ca(II) complex groups received respective compound dosage. All of the groups received 1% carrageenan solution in sub-plantar region of right paw. Thickness of rat paws measured by water displacement after 5 min ($t_o = 0$) exhibited the initial paw volume. The thickness of paw volume was measured after 1, 2, 3, 4 and 5 h.

Histamine- and PGE_2-Induced Paw Edema The anti-inflammatory mechanism of synthesized Ca(II) complex was evaluated using the histamine- and prostaglandin E2 (PGE_2)-induced paw edema assays. The SD rats were randomly divided into five groups ($n = 6$): the histamine or PGE_2 group, low (5 mg/Kg), medium (10 mg/Kg) and high (20 mg/Kg) dose Ca(II) complex groups and standard meloxicam (10 mg/Kg) group [31]. Rats in the histamine or PGE_2 group received 1 mL oral gavage of 0.5% CMC and served as inflammatory control group, while rats in standard meloxicam and low, medium and high dose Ca(II) complex groups received respective compound dosage. After 1 h, paw edema was induced by sub-planter injection of 0.1 mL of histamine (1 mg/mL) or prostaglandin E2 (0.01 μg/mL). Paw volume of each rat was immediately measured before and

after the sub-planter administration of inflammatory agents at 1, 2, 3 and 4 h [32].

Acetic Acid-Induced Analgesic Potential Acetic acid-induced writhing test was performed to evaluate the analgesic potential of meloxicam and its Ca(II) complex. The rats were randomly divided into three groups ($n = 6$): acetic acid control group (0.5% CMC), Ca(II) complex (10 mg/Kg)- and meloxicam (10 mg/Kg)-treated groups. Rats in both the meloxicam and complex group (10 mg/Kg body weight) were administered orally as a suspension in 0.5% CMC, to 16 h fasten rats. Later, upon 1 h of treatment, 0.6% acetic acid (10 mL/Kg) was injected intraperitoneally to induce the characteristic writhing in the rats. The number of writhings occurring between 5 and 25 min after the acetic acid injection in control and treated animals was recorded. The anti-nociceptive activity of drugs was calculated by the following formula.

$$\text{Percentage inhibition of writhing} = ((\text{mean writhing of control - mean writhing of test /mean writhing of control}) \times 100$$

2.5 In-Silico Molecular Docking Study

The in silico molecular docking was studied by preparing and optimizing the three-dimensional structure of the drugs meloxicam, diclofenac sodium and calcium complex in software Avogadro, respectively [33]. The protein receptors COX-1 and COX-2 were downloaded from RCSB PDB (ID: 1CQE and 6COX, respectively). The binding pockets of COX-2 and amino acids lining the cavity were identified using software Deepsite-PlayMolecule [34]. The receptor and ligand files were subjected to Patchdock Beta 1.3 software for docking [35, 36]. The docking scores, approximate interface protein–ligand complex area and values of atomic contact energy (ACE) (kJ/mol) were recorded for the proposed inhibitor ligands. The docking mode of enzyme inhibition was selected, and the root-mean-square deviations of atomic positions were 1.5 [37]. The results were analyzed by using UCSF Chimera 1.14 [38].

2.6 Statistical Analysis

Statistical analyses were performed using one-way ANOVA with Tukey test by GraphPad prism (version 7.03). Data for in vivo study were presented as mean ± SEM values. P value < 0.05 was accepted as statically significant.

3 Results and Discussion

3.1 Synthesis of Ca(II) Complex of Meloxicam

The synthesis of calcium complex of meloxicam was accomplished by mixing ethanolic solutions of meloxicam and $CaCl_2$ at pH 7 (Fig. 2). The inert nature of calcium required overnight stirring of the mixture; afterward, the pale white precipitates were obtained after heating the mixture at 60 °C.

The UV–visible absorbance peaks shifted to 375 and 280 nm for Ca(II) complex from 365 and 275 nm of the ligand, respectively. This shifting showed the involvement of meloxicam in complexation with calcium (Fig. 3a). The UV–Vis spectra of the complex did not change on keeping the DMSO solutions for 48 h, and no precipitation, turbidity or decomposition were observed even after long storage at room temperature (at least 3 months after preparation). This clearly indicates the stability of Ca(II) complex. ^{13}C NMR spectra in DMSO-D_6, δ ppm, showed suppression of peaks in C=O and C–OH region (Fig. 3b). The ^{13}C NMR of meloxicam shows definitive peaks in region > 150 ppm as reported in literature [39]. The diminishment of peaks in 156 and 160 ppm ranges reported for meloxicam in the literature depicts the formation of complex through these groups [40]. The FTIR spectra of meloxicam depicted prominent absorption bands at 3282(sh, s) cm^{-1}, 1614(sh, s) cm^{-1}, 1550 (s) cm^{-1}, 1342(s) cm^{-1} and 1182(s) cm^{-1} which can be attributed to the stretching vibrations of $\nu(N–H)_{amide}$, $\nu(C=O)_{amide}$, $V(C=N)_{thiazolyl\ ring}$, $\nu(SO_2)_{asym}$ and $\nu(SO_2)_{sym}$, respectively (Fig. 3c). The FTIR results of synthesized Ca(II) complex showed no absorption peaks in the region of 3200–3300 cm^{-1} relating to N–H stretching mode because the N–H group of meloxicam is involved in a strong intramolecular hydrogen bond to enolate oxygen. The bands of stretching vibrations for the $\nu(C=O)_{amide}$ and $V(C=N)_{thiazolyl\ ring}$ are shifted to lower wavenumber in the spectra of the Ca(II) complex which indicates the coordination of H_2mel through these two groups [21, 41]. In comparison with the meloxicam spectrum, the two stretching bands of the SO_2 group (ν_{as} and ν_s) also shift slightly to lower frequencies (Fig. 3d). Flame emission spectroscopy results showed complete absence of sodium metal, while the atomic absorption spectroscopy showed the incorporation of calcium in our synthesized Ca(II) Complex.

3.2 FESEM and EDS Analysis

FESEM was employed to study surface and structural morphology of synthesized Ca(II) complex of meloxicam. The SEM images of Ca(II) complex revealed perfectly crystalline morphology (Fig. 4a) with rectangular-shaped crystals, while uncoordinated meloxicam has rock-like morphology, with irregularly shaped crystals of various sizes [42]. SEM analysis depicted significant changes in the shape and surface

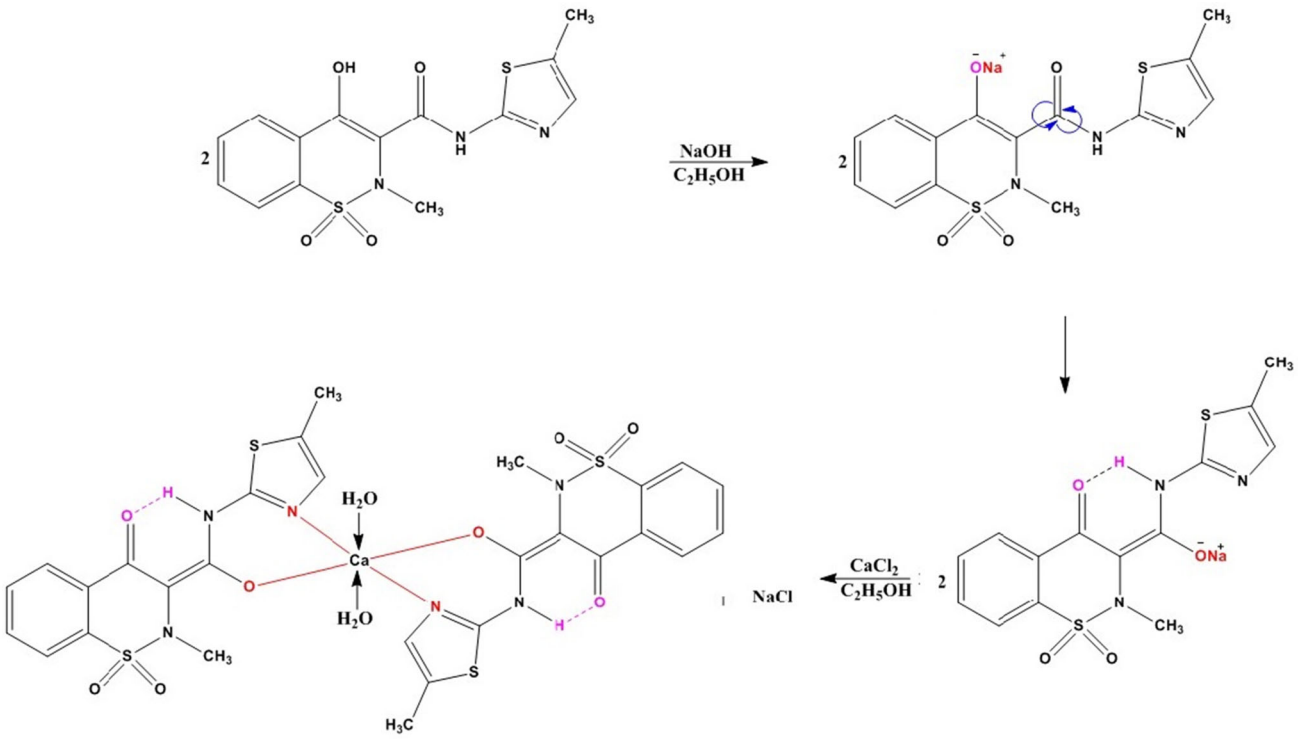

Fig. 2 Synthesis scheme for Ca(II) meloxicam complex

morphology of Ca(II) complex which occurred due to the complexation, and it might improve the properties of meloxicam. The cavities in the crystal system could be used for the electrostatic drug loading [22]. The EDS is used to calculate the percentage level of the elements present in the metal complexes like C, O, N, S and respective metal present in the complex [43]. This result confirms the presence of calcium along with other elements in the synthesized complex (Fig. 4b). The revealed data are in good agreement with that of the elemental analysis.

3.3 Powder XRD Analysis

The crystallinity of Ca(II) complex of meloxicam was evaluated by powder XRD measurement. The X-ray diffractogram of Ca(II) complex exhibited several sharp peaks at different angles (2θ) 8.04, 9.08, 12.56, 15.04, 16.72, 17.08, 18.28, 19.52, 20.4, 21.96 and 28.4° suggested that the synthesized Ca(II) complex existed as crystalline material (Fig. 5), while the X-ray diffractogram of pure meloxicam exhibited sharp peaks at different angles (2θ) 13.0, 15.0, 18.5 and 26.0° [44]. It is observed from X-ray diffractogram that complexation of meloxicam with calcium metal enhanced its crystallinity. The average crystalline sizes of the Ca(II) complex (d_{XRD}) were calculated using Debye–Scherrer equation ($D = K\lambda/\beta$ Cos θ), where D = particle size, K = dimensionless shape factor, λ = X-ray wavelength (0.15406 Å), β = full width at half maximum (FWHM) of the diffraction peak, and θ = diffraction angle [45]. The synthesized Ca(II) complex has a crystalline size of 32.86 nm suggesting that the complex is in a nanocrystalline phase.

3.4 Thermogravimetric Analysis

Thermogravimetric analyses (TGAs) are used to get information about the thermal stability of new complexes and suggested a general scheme for their thermal decomposition [46]. The TGA results depicted the degradation of Ca(II) complex in three steps. The mass (7.34%) loss for water molecules was found in first step of degradation at T_{max} 190 °C. In the second step of degradation, 48.91% mass was lost due to ethene and nitrous oxides of the organic ligand at T_{max} 261, 288 °C. The third step of degradation was recorded at T_{max} 566 °C owing to the decomposition of second ligand moiety, and $CaCO_3$ was the final decomposition product with some residual carbon about 0.024 g (Fig. 6). The activation energy (E_α = 323.84 kJ/mol) value for Ca(II) complex was calculated by Coats Redfern equation, which shows a high thermal stability of the complex [23].

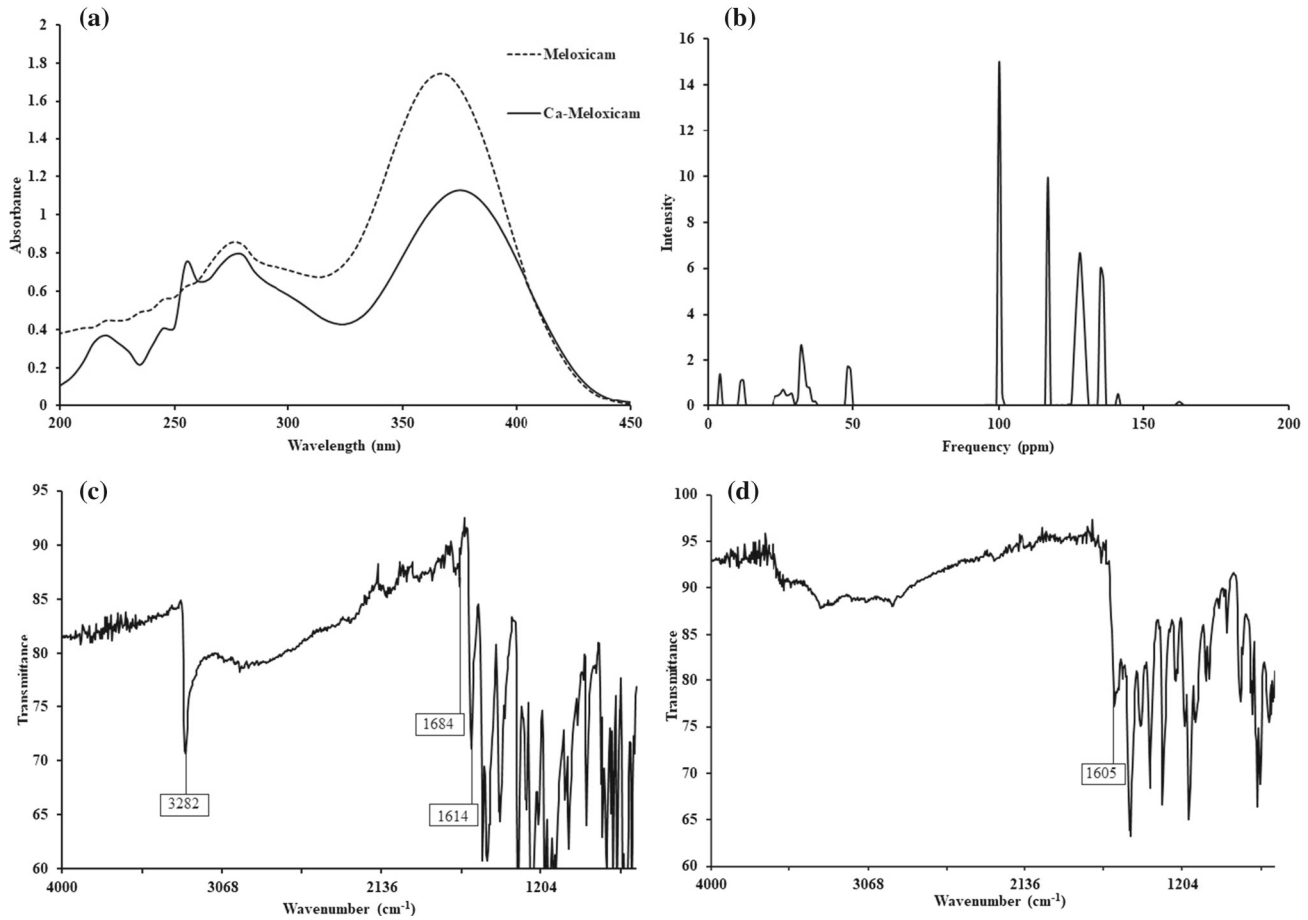

Fig. 3 Characterization of Ca(II) complex **a** UV–visible spectrophotometry of meloxicam and Ca(II) complex of meloxicam, **b** ^{13}C NMR of Ca(II) complex, **c** FTIR spectra of meloxicam, **d** FTIR spectra of Ca(II) complex

3.5 Biological Evaluation

3.5.1 Antioxidant Assays

The free radical scavenging, metal chelating and reducing abilities of meloxicam and its synthesized Ca(II) complex determined by using five different in vitro assays as more than one method are used to evaluate the antioxidant capacity/activity of a desired sample [47]. The radical scavenging, metal chelating and reducing capabilities of compounds were summarized in the form of IC_{50} values (Table 1). DPPH and ABTS radical scavenging activity has been widely used to test the ability of compounds to act as free radical scavengers or hydrogen donors and thus to evaluate the antioxidant activity [48]. The ABTS assay is better than DPPH as ABTS is soluble in water and organic solvents, and it reacts relatively rapidly with the tested compounds compared to DPPH [49]. The tested compounds interact with the stable free radical DPPH which shows their radical scavenging ability. This interaction was found to be concentration and time dependent, but the IC_{50} values of meloxicam and its Ca(II) complex were higher; > 2000 μM, while in ABTS radical scavenging assay, Ca(II) complex showed prominent radical scavenging potential in a concentration-dependent manner as compared to meloxicam and standard ascorbic acid. The IC_{50} values for ABTS radical scavenging of Ca(II) complex, meloxicam and standard ascorbic acid showed decreasing trend with respect to time, and lowest IC_{50} values were recorded at 120 min: 44.8, 82.22 and 104.12 μM, respectively. Meloxicam itself has anti-radical properties and has been reported to reduce the formation of reactive oxidants [50], but complexation with calcium metal enhanced its ABTS radical scavenging properties.

Iron chelating activity is based on the absorbance measurement of iron (II)–phenanthroline complex. This complex produced a red chromophore with a maximum absorbance at 512 nm [51]. The synthesized compounds act as chelating agents and capture the ferrous ion (Fe^{2+}) before phenanthroline. This method is used to determine the extent of Fe^{2+} + chelation by meloxicam and its Ca(II) complex. It was found that IC_{50} values of meloxicam were much lower as compared to its Ca(II) complex showing its greater Fe^{2+} chelating abil-

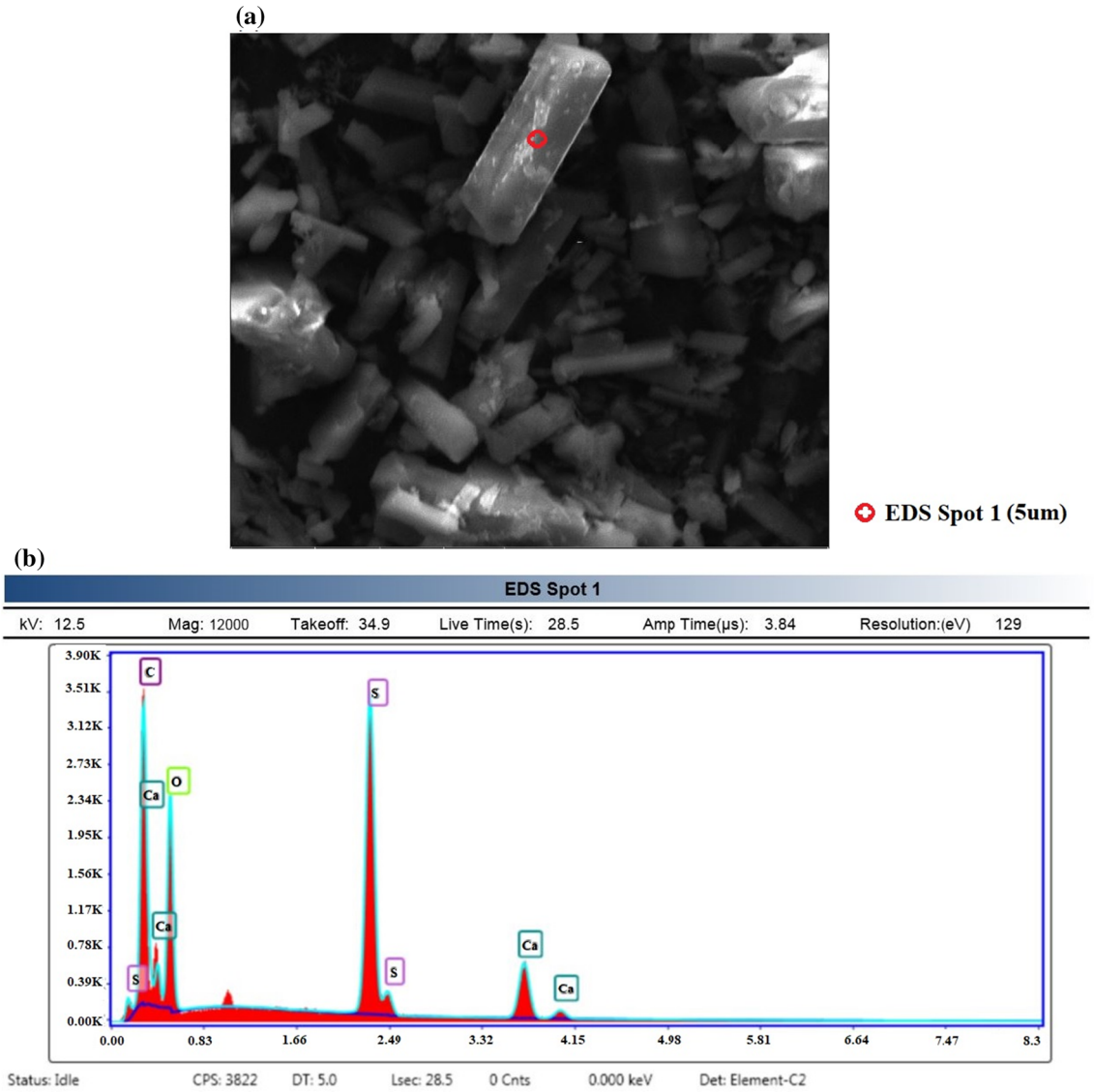

Fig. 4 **a** Field emission scanning electron microscope (FESEM) images of Ca(II) complex at 5 µm, **b** energy-dispersive spectroscopy (EDS) of the spot-1 of Ca(II) Complex crystal

ity. Higher IC_{50} value (>2000 µM at 120 min) of Ca(II) complex corresponds to its lower chelating ability, which might be due to complexation as meloxicam is already in complexed form with calcium. It might be possible that the moieties of meloxicam responsible for chelating Fe^{2+} are now involved in complexation with calcium metal and therefore exhibited lower iron chelating activity.

In $FeCl_3$ reducing power assay, meloxicam and its Ca(II) complex reduced potassium ferricyanide (Fe^{3+}) to potassium ferrocyanide (Fe^{2+}) which then reacted with ferric chloride to form ferric ferrous complex [52]. In this assay, IC_{50} of Ca(II) complex was found to be lower than un-coordinated meloxicam at all time intervals. Lower IC_{50} values indicate a higher antioxidant power of Ca(II) complex to reduce Fe^{3+} to Fe^{2+}. So, it is observed that complexation of meloxicam with calcium enhanced its iron reducing capabilities but lowers iron chelating capacity. Similarly, phospho-molybdenum (PM) activity is based on the reduction of Mo (VI) to Mo (V) by the test compounds, giving a direct approximation of reducing capacity of the compounds [53]. Similar results were observed in PM activity, and IC_{50} of Ca(II) complex was found to be lower than meloxicam and ascorbic acid, indicating higher reducing activity of meloxicam in complex form. From the overall results, it is concluded that the Ca(II) complex of meloxicam exhibited potent radical scavenging and reducing abilities in ABTS, $FeCl_3$ reducing power and phospho-molybdenum antioxidant assays than uncoordinated meloxicam. The Ca(II) complex of meloxicam did not show promising iron chelating ability which is the indication of complexation between meloxicam and calcium.

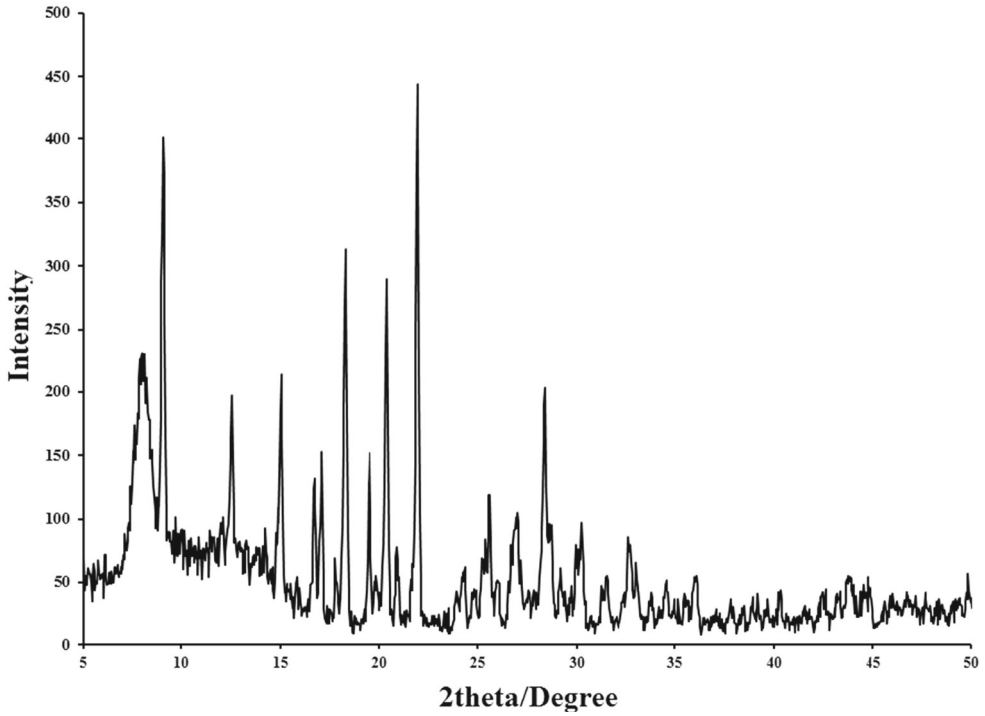

Fig. 5 Powder X-ray diffraction (XRD) patterns of Ca(II) complex of meloxicam

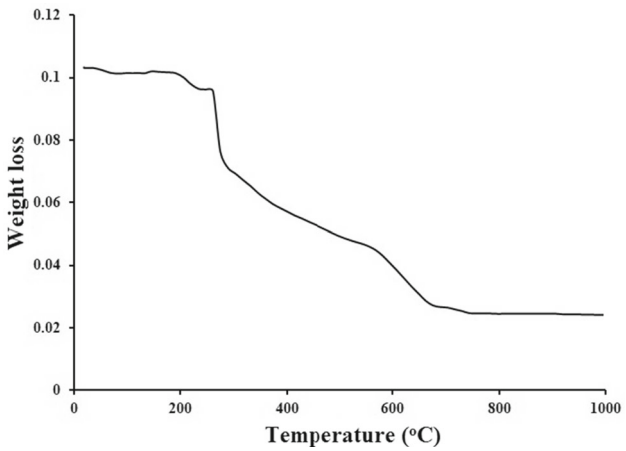

Fig. 6 Thermogravimetric analysis (TGA) of Ca(II) complex

3.5.2 In Vitro Cyclooxygenase Inhibitor Assay

The COX-1/2 inhibitory activities of the synthesized Ca(II) complex were evaluated and compared with free meloxicam using the enzyme immunoassay (EIA) method against ovine COX-1 and human recombinant COX-2. The half maximal inhibitory concentration IC_{50} values calculated from experimental data are shown in Table 2. The selectivity index was calculated as the ratio IC_{50} COX-1/IC_{50} COX-2. The results obtained for the standard NSAIDs meloxicam are similar to those described by the previous studies [26, 54]. The tested Ca(II) complex showed half maximal inhibitory concentration for COX-1 by concentrations of 211.95 μM, while for COX-2 half inhibitory concentration is achieved by concentrations as low as 4.84 μM. The Ca(II) complex and meloxicam both have a potent COX-2 inhibitory effect with IC_{50} < 30 μM. When considering the selectivity index as well as the inhibitory potency, the Ca(II) complex was proved to be more selective toward COX-2, as compared to meloxicam. According to Warner et al., selectivity indices ranging from 5 to 50 are associated with compounds that markedly inhibit more the COX-2 isoform than COX-1 and represent the ideal range for the development of safe and selective COX-2 inhibitors [55]. This Ca(II) complex can be considered as a selective COX-2 inhibitor as it showed 43.77 selectivity index (SI) toward COX-2, while meloxicam with 10.39 selectivity is considered as preferential COX-2 inhibitor [56].

3.5.3 Acute Toxicity of Ca(II) Complex of Meloxicam

Before the in vivo evaluation, we evaluated the toxicity of Ca(II) complex to demonstrate safety and their safe dose [27]. The results suggested that the oral LD_{50} of Ca(II) complex is 1000 mg/Kg (Table 3, rats = 10). The toxicity of Ca(II) complex appeared to be much lower than the toxicity of the reference drug meloxicam. The LD_{50} threshold for oral meloxicam is 470 mg/Kg [57, 58]. According to OECD guidelines for acute oral toxicity, an LD_{50} dose of > 300–2000

Table 1 IC_{50} values for antioxidant activities of Ca(II) complex and meloxicam

Activity	Compounds	IC_{50} values (μM) w.r.t. time (minutes)					
		5	15*	30	45	60	120
DPPH	Ca(II) Complex	–	>2000	>2000	>2000	>2000	>2000
	Meloxicam	–	>2000	>2000	>2000	>2000	>2000
	Ascorbic acid	–	214.25	219.27	231.21	242.36	240.17
ABTS	Ca(II) Complex	84.1	68.2	58.4	53.9	51.6	44.8
	Meloxicam	124.74	95.72	88.92	85.90	81.77	82.22
	Ascorbic acid	138.29	131.24	125.17	120.85	117.79	104.12
Iron chelating	Ca(II) Complex	–	15	408.55	>1000	>1000	>2000
	Meloxicam	–	9.8	11.3	12.0	12.2	15.9
	Ascorbic acid	–	4.34	3.25	1.43	1.55	1.44
$FeCl_3$ reducing power	Ca(II) Complex	–	5.25	5.55	5.9	6.05	4.8
	Meloxicam	–	7.8	8.05	8.4	8.7	9.6
	Ascorbic acid	–	15.64	15.74	14.22	13.36	12.44
Phospho-molybdenum	Ca(II) Complex	–	32.8	37.7	36.98	31.8	–
	Meloxicam	–	55.2	50.6	56.8	59.8	–
	Ascorbic acid	–	45.62	56.55	58.06	57.43	–

*10 min for iron chelating and $FeCl_3$ reducing power activity

Table 2 Experimental IC_{50} (μM) against COX-1 and COX-2 for Ca(II) complex

Compounds	IC_{50} (μM)		Selectivity index (SI)
	COX-1	COX-2	
Ca(II) complex	211.95	4.84	43.77
Meloxicam	138.16	13.28	10.39

Table 3 Animal group specification and drug dose administered for acute toxicity of Ca(II) complex

Groups	Rats		Ca(II) complex (mg/kg b.wt)
	Male (Survived)	Female (Survived)	
1	5 (5)	5 (5)	5
2	5 (5)	5 (5)	25
3	5 (5)	5 (5)	50
4	5 (5)	5 (5)	100
5	5 (5)	5 (5)	250
6	5 (5)	5 (5)	500
7	5 (3)	5 (2)	1000
8	5 (0)	5 (0)	2000

is categorized as category 4 and hence the drug is found to be safe. The extended safety index of Ca (II) complex of meloxicam is probably related to the complexation of Calcium with meloxicam through amide oxygen and thiazolyl ring nitrogen.

3.5.4 In Vivo Anti-Inflammatory Activity

To evaluate the in vivo anti-inflammatory potential of synthesized Ca(II) complex at different doses (5, 10, 20 mg/Kg), the carrageenan-induced paw edema method was employed (Fig. 7). It was found that meloxicam and its Ca (II) complex showed a significant anti-inflammatory effect by reducing the paw volume after 2 h of activity, while the paw volume of carrageenan group rats was at peak after 3 h. The Ca (II) complex at 10 mg/Kg showed significant reduction in paw volume ($^*P < 0.05$) followed by its 20 mg/Kg dosage and standard meloxicam, while Ca (II) complex at 5 mg/Kg exhibited the least response.

The development of edema induced by carrageenan is biphasic: The first phase occurs within 1 h of carrageenan inflammation and is attributed to the release of the neurotransmitter molecules histamine and serotonin. The second phase (over 1 h) is mediated by an increased release of prostaglandins in the inflammatory area, and the continuity between the two phases is provided by kinins [59]. After 3 h of activity, carrageenan group rats exhibited maximum swelling and redness in inflamed paw as compared to other treated groups which was scored from 0–4 on the basis of severity (Fig. 8). In scoring, 0 was assigned to normal; 1 represented minimal inflammation and edema of injected paw; 2 was denoted to mild paw inflammation and edema; 3 was allocated to moderate inflammation and edema; and 4 was assigned to severe inflammation and redness of paw.

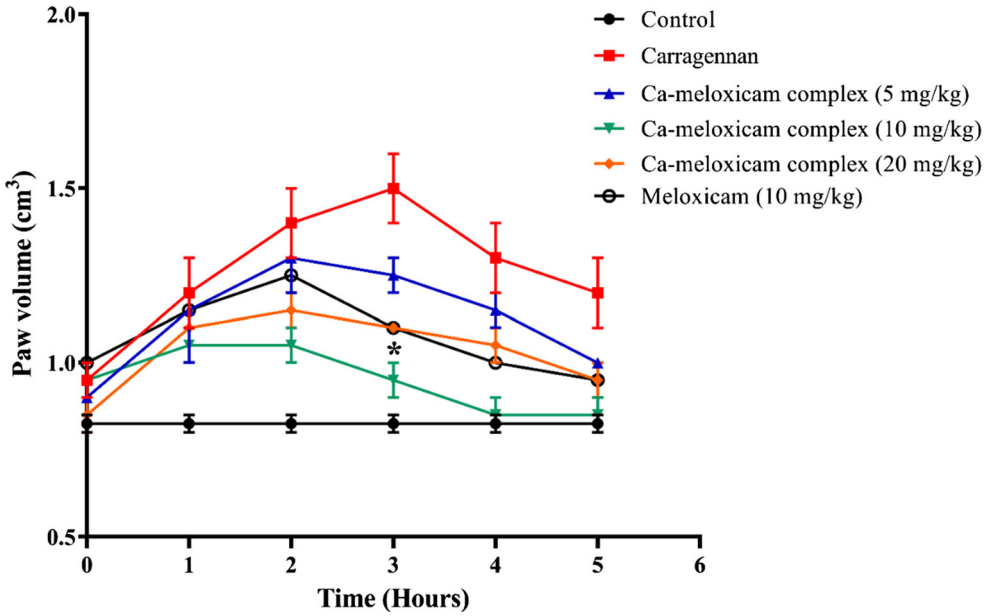

Fig. 7 In vivo anti-inflammatory activity by carrageenan-induced paw edema of Ca(II) complex (5, 10 and 20 mg/Kg) and meloxicam (10 mg/Kg). $^*P < 0.05$ shows statistical difference between carrageenan and Ca(II) complex (10 mg/Kg) group. All the values are represented as Mean ± SEM

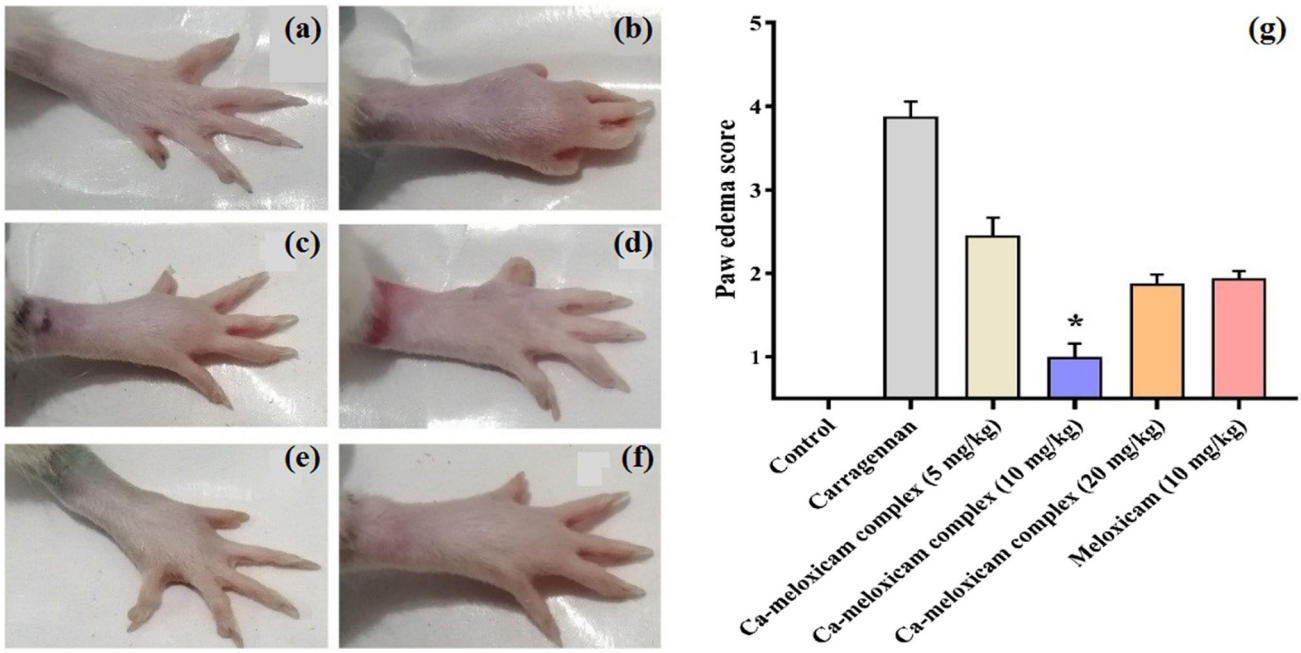

Fig. 8 Carrageenan-induced paw edema after 3 h of activity **a** normal paw, **b** inflamed paw, **c** Ca(II) complex (5 mg/Kg)-treated paw, **d** Ca(II) complex (10 mg/Kg)-treated paw, **e** Ca(II) complex (20 mg/Kg)-treated paw, **f** meloxicam (10 mg/Kg)-treated paw and **g** paw edema score according to following criteria: 0 was assigned to normal; 1 represented minimal inflammation and edema of injected paw; 2 was denoted to mild paw inflammation and edema; 3 was allocated to moderate inflammation and edema; and 4 was assigned to severe inflammation and redness of paw. Data are presented as Mean ± SEM

3.5.5 Histamine-Induced Paw Edema

Histamine-induced inflammation has been well established as a valid model to study paw edema because histamine evokes the release of neuropeptides and prostaglandins from endothelial cells leading to hyperalgesia [60, 61]. Rats of histamine-induced paw edema group showed rise in paw volumes after 1, 2 and 3 h of sub-plantar injection of histamine

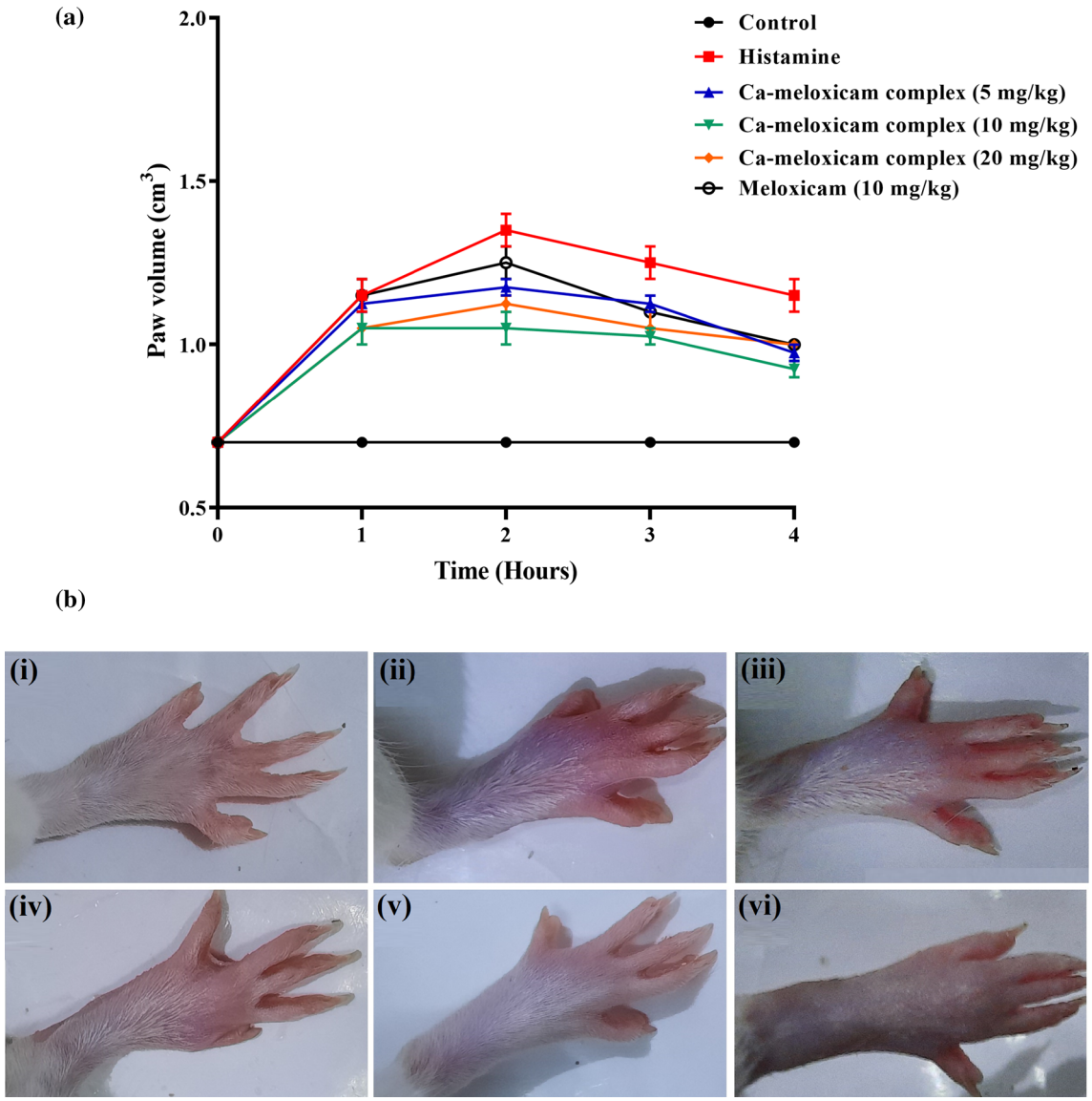

Fig. 9 In vivo anti-inflammatory activity by histamine-induced paw edema, **a** paw volume of control, histamine, Ca(II) complex (5, 10 and 20 mg/Kg) and meloxicam (10 mg/Kg) group rats. All the values are represented as Mean ± SEM, **b** redness and paw edema after 2 h of activity (i) normal paw, (ii) histamine-induced inflamed paw, (iii) Ca(II) complex (5 mg/Kg)-treated paw (iv) Ca(II) complex (10 mg/Kg)-treated paw, (v) Ca(II) complex (20 mg/Kg)-treated paw, (vi) meloxicam (10 mg/Kg)-treated paw

compared with the paw volume of rats of the untreated control group (Fig. 9a). Rats pretreated with oral Ca(II) complex and meloxicam showed slight decrease in paw volumes after 2 h. There was no significant difference between paw volumes among the treated groups, but Ca(II) complex at 10 mg/Kg showed prominent response at 2, 3 and 4 h (Fig. 9a). After 2 h of activity, histamine group rats exhibited maximum swelling and redness in the inflamed paw as compared to other treated groups (Fig. 9b). Inflammation likely consists of three stages; an increase in vascular permeability; leukocyte migration; and proliferation of connective tissue. Swelling is the first stage in the inflammatory process. Although the second stage of inflammation is not dependent on the first stage, the therapeutic effects of agents acting on the second stage may be influenced by the first stage [61].

3.5.6 PGE_2-Induced Paw Edema

PGE_2 is a very important mediator of all types of inflammation and is responsible for increased prostaglandin production in inflamed tissue [62]. Rats of PGE_2-induced paw edema group showed rise in paw volumes after 1 and 2 h of sub-plantar injection of PGE_2 compared with the paw volume of rats of the untreated control group (Fig. 10a). Rats

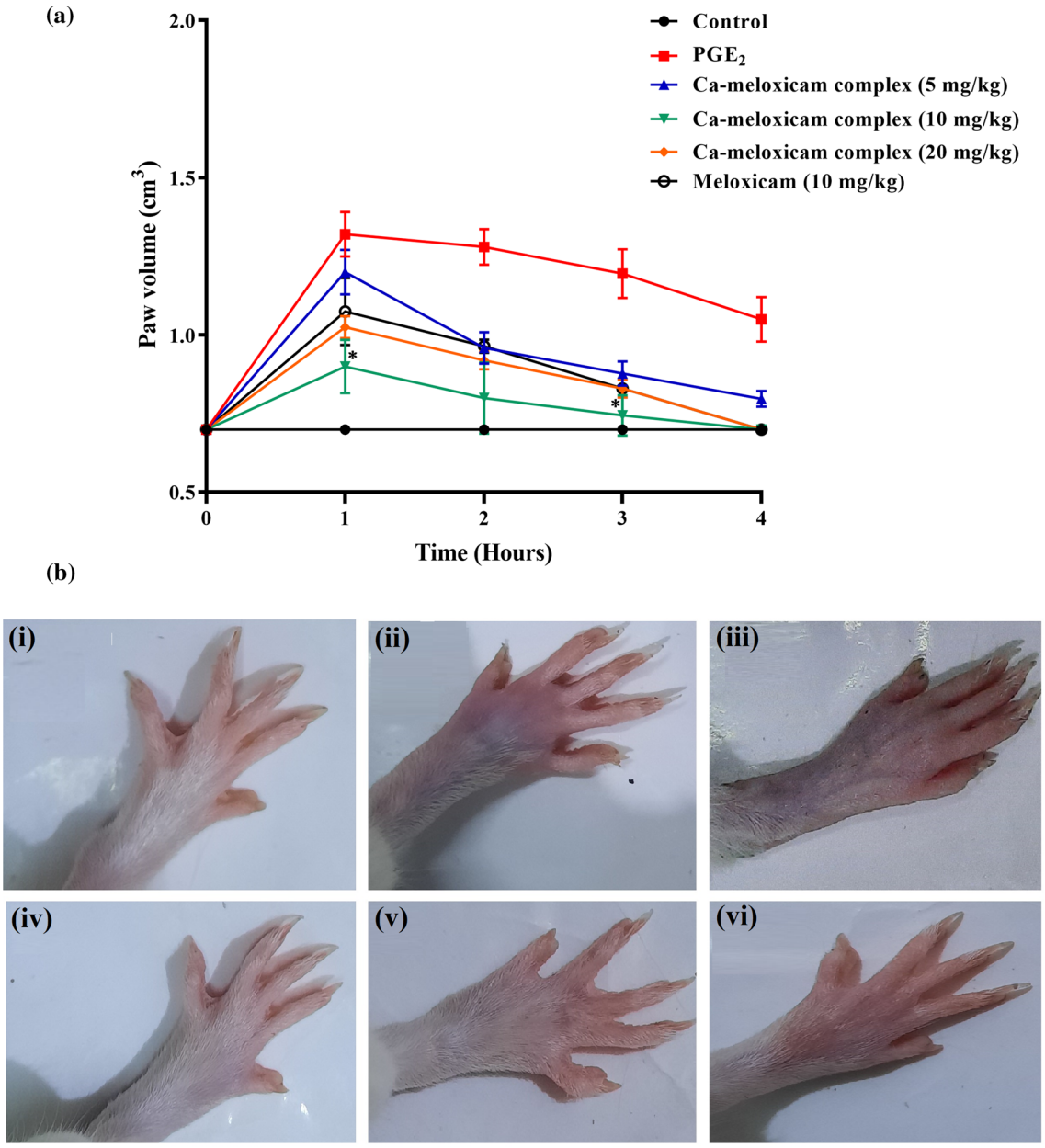

Fig. 10 In vivo anti-inflammatory activity by PGE_2-induced paw edema, **a** paw volume of control, PGE_2, Ca(II) complex (5, 10 and 20 mg/Kg) and meloxicam (10 mg/Kg) group rats. $^*P < 0.05$ shows statistical difference between PGE_2 and Ca(II) complex (10 mg/Kg) group, all the values are represented as Mean ± SEM. **b** Redness and paw edema after 2 h of activity (i) normal paw, (ii) PGE_2-induced inflamed paw, (iii) Ca(II) complex (5 mg/Kg)-treated paw, (iv) Ca(II) complex (10 mg/Kg)-treated paw, (v) Ca(II) complex (20 mg/Kg)-treated paw, (vi) meloxicam (10 mg/Kg)-treated paw

pretreated with oral Ca(II) complex at 10 mg/Kg showed significant decrease in paw volumes after 1 h of activity ($P < 0.05$). All the treated group showed decrease in paw volume, but Ca(II) complex at 10 mg/Kg showed significant response at 1, 2, 3 and 4 h (Fig. 10a). After 2 h of activity, PGE_2 group rats exhibited maximum swelling and redness in the inflamed paw as compared to other treated groups (Fig. 10b). Our results indicated that Ca(II) complex was more potently inhibited PGE_2-induced paw edema than meloxicam at similar doses (10 mg/Kg). In the prostaglandin (PGE_2) biosynthesis pathway, (COX-2) is the key enzyme that catalyzes the conversion of arachidonic acid to PGE_2 [63] and this finding was confirmed by our observation in the in vitro inhibition of COX-2 by Ca(II) complex. These results indicate that the inhibitory effect of Ca(II) complex on carrageenan edema is probably due to PGE_2 reduction

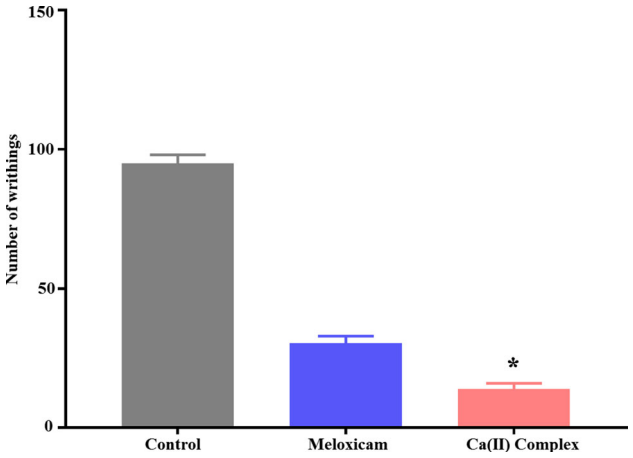

Fig. 11 Analgesic activity by acetic acid-induced writhing test of Ca(II) complex (10 mg/Kg) and meloxicam (10 mg/Kg). *P <0.05 shows statistical difference between control and Ca(II) complex group. Values are expressed as the mean ± SEM

Table 4 Effect of Ca(II) complex on the number of writhing responses in acetic acid-induced writhing analgesic activity

Groups	N	Writhing response	% Inhibition of writhing
Control	6	95 ± 4.24	–
Meloxicam (10 mg/Kg)	6	30.5 ± 3.54	67.89
Ca(II) complex (10 mg/Kg)	6	14 ± 2.83*	85.26

*P <0.05 shows statistical difference between control and Ca(II) complex group. Values are expressed as the mean ± SEM

since its effect on carrageenan edema was more pronounced than that one produced by histamine.

3.5.7 Acetic Acid-Induced Analgesic Potential

Acetic acid-induced writhing test was used to evaluate the analgesic potential of meloxicam and its Ca(II) complex at 10 mg/Kg. Acetic acid-induced writhing test is a model of peripheral pain that is useful for anti-nociceptive drug development [64]. The Ca(II) complex showed more significant response (*P <0.05) and reduced the number of characteristic writhing in rats as compared to meloxicam (Fig. 11). Consequently, highest percentage (85.26%) inhibition of writhing response was produced by Ca(II) complex at 10 mg/Kg, while meloxicam showed 67.89% inhibition (Table 4). NSAIDs act by the reduction of sensitization of pain receptors caused by prostaglandins at the inflammation site [65].

3.6 In Silico Molecular Docking Study

The molecular docking study was performed in order to investigate the binding interaction of Ca(II) complex at the binding/active site of COX-1 and COX-2 protein (PDB code: 1CQE and 6COX, respectively) [66, 67]. The software Deepsite-PlayMolecule helped to assess the binding sites in the three-dimensional structure of enzymes (Fig. 12).

The molecular docking was performed according to the given literature for binding pocket of COX enzymes containing THR_{118}, ARG_{120}, GLN_{192}, VAL_{349}, TYR_{355}, GLU_{364}, PHE_{518}, VAL_{523} (ILE_{523} in COX-1), ALA_{527}, MET_{535}. Structural differences among the binding sites of COX-1 and COX-2 provided valuable guidelines for the design of selective COX-2 inhibitors [68, 69]. The main difference consists in the existence of a second pocket inside of COX binding site, which is more accessible in COX-2 because of the replacement of ILE_{523} in COX-1 with a smaller side chain residue VAL_{523}, linked with conformational changes at TYR_{355}, which opens the hydrophobic chain of the additional pocket including LEU_{352}, SER_{353}, TYR_{355}, PHE_{518} and VAL_{523} [70]. Meloxicam showed close interaction with VAL_{116}, LEU_{359}, LEU_{352}, SER_{353}, GLU_{524}, TRP_{387}, LEU_{384}, TYR_{385}, GLY_{526}, ALA_{527}, respectively. The two residues LEU_{352} and SER_{353} of hydrophobic chain showed interactions with meloxicam and thus account for the selectivity of meloxicam for COX-2. The docking score, approximate area of interface and ACE of meloxicam were found as 5150, 643.2 and − 281.06 kJ/mol for COX-2 and 4350, 565.1 and − 280.03 kJ/mol for COX-1, respectively. Diclofenac sodium showed the parameters as 5054, 621.10 and − 121.24 kJ/mol for COX-2 while 4336, 474.7 and − 113.5 kJ/mol for COX-1, respectively. The Ca(II) complex showed close hydrophobic interaction with LEU_{80}, LEU_{81}, LEU_{82}, LYS_{83}, VAL_{89}, ARG_{120}, TRY_{122}, SER_{471}, LEU_{472}, LYS_{473}, SER_{119}, VAL_{523} and GLU_{524} with docking score, approximate area of interface and ACE as 6438, 857.6 and − 289.87 kJ/mol for COX-2 (Fig. 13a and b) while 5732, 767.2 and − 193.77 kJ/mol for COX-1, respectively (Fig. 13c and d). The highly negative ACE values depict greater potential of formation of the enzyme–inhibitor complex due to exothermic energy change. The Ca(II) complex fitted well into COX-2 binding site occupying a similar but greater region in the binding site as meloxicam. This pose might benefit from additional interaction energy due to the relative proximity of the VAL_{116}, which can generate an additive effect determining the selectivity for COX-2 [71].

The docking of Ca(II) complex revealed intricate interactions with COX-2 channel, including hydrogen bonds and hydrophobic interactions having highest dock/binding score compared to meloxicam. Furthermore, it was observed previously that the compounds having higher selectivity index (SI) for COX-2 than COX-1 in the in vitro experiments also

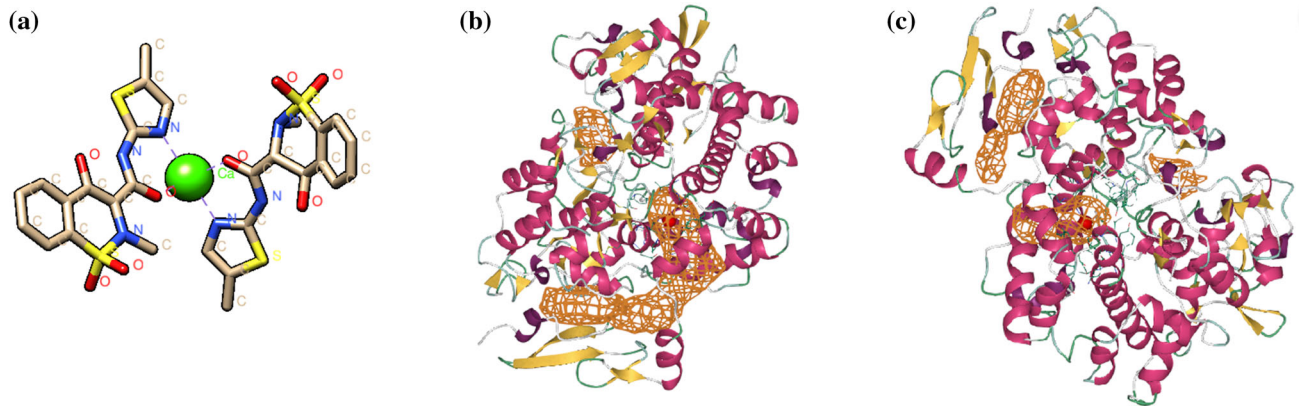

Fig. 12 3D structures of Ca(II)-complex and COX enzymes, **a** optimized structure of Ca(II)-complex, **b** binding pockets of COX-1 (PDB ID: 1CQE) and **c** binding pockets of COX-2 (PDB ID: 6COX)

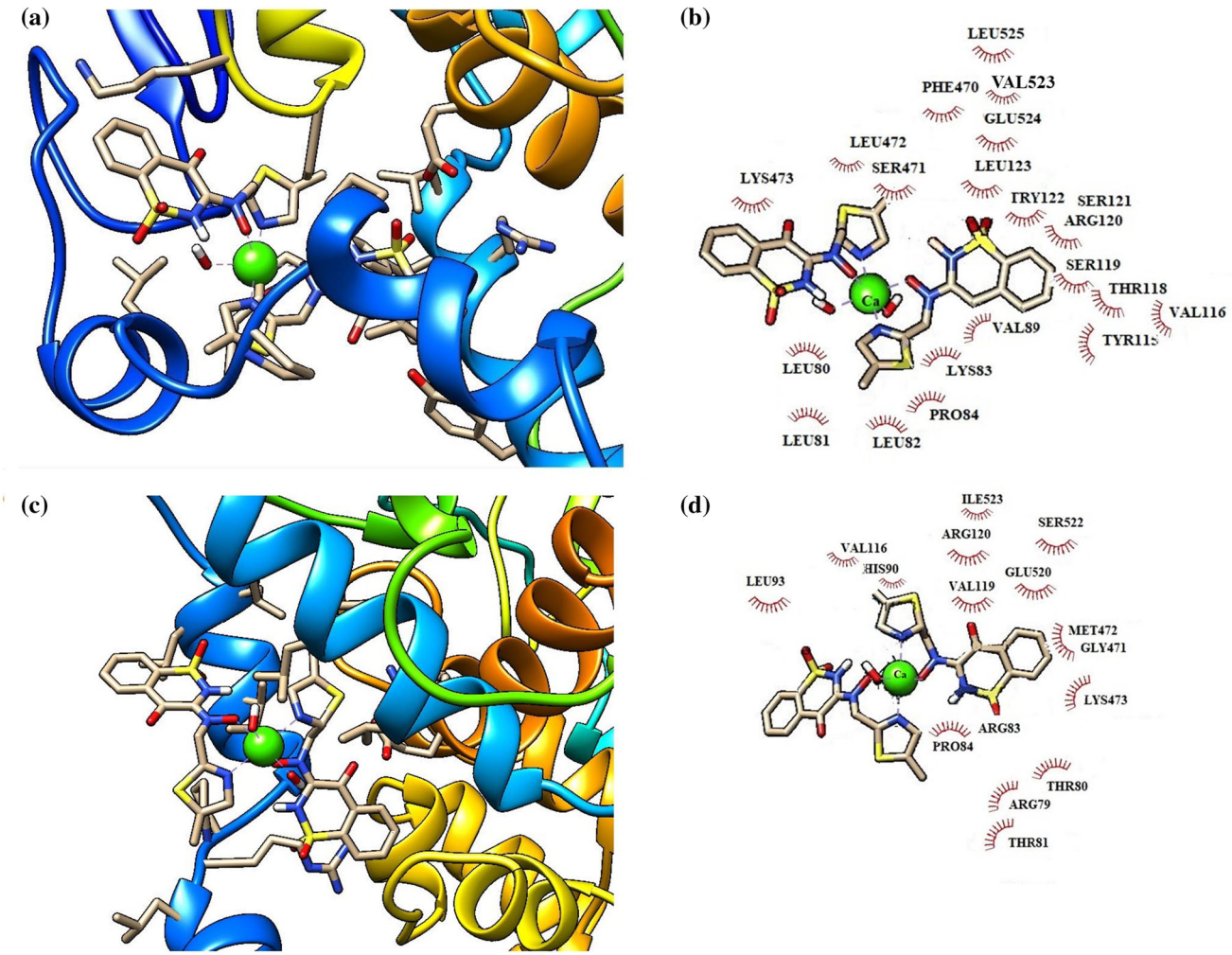

Fig. 13 Molecular docking interactions of Ca(II) complex with COX enzymes **a** 3D interactions of Ca(II) complex with COX-2, **b** 2D interactions of Ca(II) complex with COX-2, **c** 3D interactions of Ca(II) complex with COX-1, **d** 2D interactions of Ca(II) complex with COX-1

showed higher binding interactions (dock score) with COX-2 than COX-1 in molecular docking studies [26, 32, 72–75]. On this basis, the compounds with higher docking score are recognized as selective COX-2 inhibitors.

4 Conclusion

A new Ca(II) complex of meloxicam was synthesized and investigated by various spectroscopic and biological techniques. The spectral studies envisaged that the meloxicam ligand is bidentate in nature, which coordinate with the Ca(II) metal ion through oxygen of amide group and nitrogen of thiazolyl ring. The correlation of the experimental data allows in assigning an octahedral geometry for the Ca(II) complex. SEM and XRD analysis showed crystalline morphology of complex and is in good agreement with each other. TGA data revealed that the complex decomposes into three steps resulting in a metal carbonate as final decomposition product. The new Ca(II) complex showed prominent in vitro antioxidant activities and higher selectivity toward COX-2 than uncoordinated meloxicam. It showed lower toxicity with LD_{50} 1000 mg/Kg and acts as a potent anti-inflammatory and analgesic agent. It inhibits PGE_2-induced inflammation more strongly than histamine which justifies the anti-inflammatory and analgesic action of complex. Molecular docking data provide new insights about COX-2 inhibitions by the new Ca(II) complex, having higher binding score as compared to COX-1, and may be considered as a potent COX-2 inhibitor. Moreover, Ca(II) meloxicam complex can be further used to explore its beneficial impacts at molecular level.

Acknowledgements This work was supported by Higher Education Commission (HEC) of Pakistan [pin # 518-85878-2PS5-066] and School of Chemistry, University of the Punjab, Lahore, Pakistan, for providing financial support and chemicals, respectively. A. Irfan would like to acknowledge the support of Deanship of Scientific Research at King Khalid University (KKU), Saudi Arabia through research groups program under grant number R.G.P.1/318/42. We should express gratitude to Aysha Siddiqa for her help in handling the animals.

Authors' Contributions MARB and MI contributed to conceptualization; MMS, AS and MARB were involved in methodology; MI, MA and IA contributed to formal analysis and investigation; AS and MMS were involved in analysis and interpretation of characterization; MMS and MARB contributed to writing—review and editing; and MARB was involved in resources and supervision.

Funding This work was supported by Higher Education Commission (HEC) Pakistan [pin # 518-85878-2PS5-066].

Declarations

Conflict of interest All the authors declare no conflict of interest. All authors have read and approved the final version of this manuscript and agree to be accountable for all aspects of work in ensuring that questions related to the accuracy or integrity of any part of the work are appropriately investigated and resolved. All persons designated as authors qualify for authorship, and all those who qualify for authorship are listed.

Ethical Approval International ethical guidelines were followed for the care of laboratory animals to provide them with a healthy and clean environment. All the in vivo experiments were approved by Institutional Ethical Committee, University of the Punjab, Lahore (Approval No. D/025/2018, March 07, 2018).

References

1. Herzberg, D.L.; Sukumaran, H.P.; Viscusi, E.: NSAIDs for analgesia in the era of COVID-19. Reg. Anesth. Pain Med. **45**(9), 677–678 (2020)
2. Sadia, A.; Basra, M.A.R.: Therapeutic dilemma in the repression of severe acute respiratory syndrome coronavirus-2 proteome. Drug Dev. Res. **81**(8), 942–949 (2020)
3. Tabas, I.; Glass, C.K.: Anti-inflammatory therapy in chronic disease: challenges and opportunities. Science **339**(6116), 166 (2013)
4. Barnes, P.J.: How corticosteroids control inflammation: quintiles Prize Lecture 2005. Br. J. Pharmacol. **148**(3), 245–254 (2006)
5. Jani, M., et al.: The role of DMARDs in reducing the immunogenicity of TNF inhibitors in chronic inflammatory diseases. Rheumatology **53**(2), 213–222 (2013)
6. Tolba, R.: Nonsteroidal anti-inflammatory drugs (NSAIDs). In: Treatment of Chronic Pain Conditions, pp. 77–79 (2017)
7. Takeuchi, K., et al.: Roles of COX inhibition in pathogenesis of NSAID-induced small intestinal damage. Clin. Chim. Acta **411**(7), 459–466 (2010)
8. Basra, M.A.R.: Impact of natural antioxidants on biological systems. LGUJLS **4**(02), 139–162 (2020)
9. Ng, S.C.; Chan, F.K.: NSAID-induced gastrointestinal and cardiovascular injury. Curr. Opin. Gastroenterol. **26**(6), 611–617 (2010)
10. Tsoupras, A.; Lordan, R.; Zabetakis, I.: Inflammation, not cholesterol, is a cause of chronic disease. Nutrients **10**(5), 604 (2018)
11. Mittal, M., et al.: Reactive oxygen species in inflammation and tissue injury. Antioxid. Redox Signal. **20**(7), 1126–1167 (2014)
12. Mouithys-Mickalad, A.M., et al.: In vitro study of the antioxidant properties of non steroidal anti-inflammatory drugs by chemiluminescence and electron spin resonance (ESR). Free Radical Res. **33**(5), 607–621 (2000)
13. Khalil, N.Y.; Aldosari, K.F.: Meloxicam. In: Profiles of drug substances, excipients and related methodology, pp. 159–197. Elsevier (2020)
14. Constantino, D.H.J.; Serotini, B.H.; Matsumoto, M.A.: Role of Meloxicam as a selective inhibitor of COX-2 in the inhibition of Ehrlich solid tumor growth. Afr. J. Pharm. Pharmacol **11**(26), 295–299 (2017)
15. Agha, A.M.; El-Khatib, A.S.; Al-Zuhair, H.: Modulation of oxidant status by meloxicam in experimentally induced arthritis. Pharmacol. Res. **40**(4), 385–392 (1999)
16. Anastassopoulou, J.; Theophanides, T.: The role of metal ions in biological systems and medicine. In: Bioinorganic chemistry, pp. 209–218. Springer (1995)
17. Dendrinou-Samara, C., et al.: Anti-inflammatory drugs interacting with Zn (II), Cd (II) and Pt (II) metal ions. J. Inorg. Biochem. **71**(3–4), 171–179 (1998)
18. Lippert B (2013) Uses of metal compounds in medicine. Ref. Module Chem. Mol. Sci. Chem. Eng.
19. Kyropoulou, M., et al.: Ni(II) complexes with non-steroidal anti-inflammatory drug diclofenac: structure and interaction with DNA and albumins. Polyhedron **61**, 126–136 (2013)

20. Medici, S., et al.: Noble metals in medicine: latest advances. Coord. Chem. Rev. **284**, 329–350 (2015)
21. Esteghamat-Panah, R., et al.: A mononuclear Ru (II) complex with meloxicam: DNA-and BSA-binding, molecular modeling and anticancer activity against human carcinoma cell lines. Inorg. Chim. Acta **454**, 184–196 (2017)
22. Kanwal, A., et al.: Synthesis and Structural Studies of Bismuth-piroxicam Complex. Rev. Chim. **69**(7), 1702–1705 (2018)
23. Sadeeket, S.A., et al.: Spectroscopic characterization, thermogravimetry, density functional theory and biological studies of some mixed-ligand complexes of meloxicam and 2,2′-bipyridine with some transition metals. Appl. Organomet. Chem. **33**(5), e4889 (2019)
24. Tajammal, A., et al.: Synthesis, antihyperglycemic activity and computational studies of antioxidant chalcones and flavanones derived from 2, 5 dihydroxyacetophenone. J. Mol. Struct. **1148**, 512–520 (2017)
25. Pham, V.C., et al.: Biological evaluation and molecular docking study of 3-(4-sulfamoylphenyl)-4-phenyl-1H-pyrrole-2, 5-dione as COX-2 inhibitor. Bull. Korean Chem. Soc. **33**(2), 721–724 (2012)
26. Oniga, S.D., et al.: COX inhibition profile and molecular docking studies of some 2-(trimethoxyphenyl)-thiazoles. Molecules **22**(9), 1507 (2017)
27. Oecd, T.N.: 425: acute oral toxicity: up-and-down procedure. OECD Guidel. Test. Chem. Sect. **4**, 1–27 (2008)
28. Randhawa, M.A.: Calculation of LD50 values from the method of Miller and Tainter, 1944. J. Ayub Med. Coll. Abbottabad **21**(3), 184–185 (2009)
29. Al-Ali, A., et al.: Oral and intraperitoneal LD50 of thymoquinone, an active principle of Nigella sativa, in mice and rats. J. Ayub Med. Coll. Abbottabad **20**(2), 25–27 (2008)
30. Moon, S.M., et al.: Oleamide suppresses inflammatory responses in LPS-induced RAW264. 7 murine macrophages and alleviates paw edema in a carrageenan-induced inflammatory rat model. Int. Immunopharmacol. **56**, 179–185 (2018)
31. Fikry, E.M.; Hasan, W.A.; Mohamed, E.G.: Rutin and meloxicam attenuate paw inflammation in mice: affecting sorbitol dehydrogenase activity. J. Biochem. Mol. Toxicol. **32**(2), e22029 (2018)
32. Jan, M.S., et al.: Design, synthesis, in-vitro, in-vivo and in-silico studies of pyrrolidine-2, 5-dione derivatives as multitarget anti-inflammatory agents. Eur. J. Med. Chem **186**, 111863 (2020)
33. Hanwell, M.D., et al.: Avogadro: an advanced semantic chemical editor, visualization, and analysis platform. J. Cheminformatics **4**(1), 1–17 (2012)
34. Jiménez, J., et al.: DeepSite: protein-binding site predictor using 3D-convolutional neural networks. Bioinformatics **33**(19), 3036–3042 (2017)
35. Schneidman-Duhovny, D., et al.: PatchDock and SymmDock: servers for rigid and symmetric docking. Nucleic Acids Res. **33**, 363–367 (2005)
36. Mashiach, E., et al.: An integrated suite of fast docking algorithms. Proteins Struct. Funct. Bioinform. **78**(15), 3197–3204 (2010)
37. Gaur, M., et al.: Molecular modeling, docking and protein-protein interaction analysis of MAPK signalling cascade involved in Camalexin biosynthesis in Brassica rapa. Bioinformation **14**(4), 145–152 (2018)
38. Pettersen, E.F., et al.: UCSF Chimera—a visualization system for exploratory research and analysis. J. Comput. Chem. **25**(13), 1605–1612 (2004)
39. Romani, L.F.A., et al.: Physicochemical characterization, the Hirshfeld surface, and biological evaluation of two meloxicam compounding pharmacy samples. J. Pharm. Anal. **8**(2), 103–108 (2018)
40. Raj, R.; Nandkishore, K.: Formulation and evaluation of meloxicam crystals using spherical crystallization for solubility enhancement. Res. Rev. J. Drug Formul. Dev. Prod. **3**, 15–35 (2016)
41. Sanatkar, T.H., et al.: The meloxicam complexes of Co (II) and Zn (II): synthesis, crystal structures, photocleavage and in vitro DNA-binding. J. Mol. Struct. **1049**, 336–344 (2013)
42. Taha, N., et al.: (2021) Anti-inflammatory and cytoprotective potentials of Meloxicam solid dispersions prepared by different techniques on lipopolysaccharide-stimulated RAW 264.7 macrophages. J. Drug Deliv. Sci. Technol. **63**, 102507 (2021)
43. Taha, R.H., et al.: Synthesis and characterization of newly synthesized Schiff base ligand and its metal complexes as potent anticancer. J. Mol. Struct. **1181**, 536–545 (2019)
44. Ghareeb, M.M., et al.: Kneading technique for preparation of binary solid dispersion of meloxicam with poloxamer 188. AAPS PharmSciTech **10**(4), 1206–1215 (2009)
45. Manjuraj, T., et al.: Synthesis, XRD, thermal, spectroscopic studies and biological evaluation of Co (II), Ni (II) Cu (II) metal complexes derived from 2-benzimidazole. J. Mol. Struct. **1171**, 481–487 (2018)
46. Mohamed, G.G.; Omar, M.M.; Hindy, A.M.: Metal complexes of Schiff bases: preparation, characterization, and biological activity. Turk. J. Chem. **30**(3), 361–382 (2006)
47. Salazar, R., et al.: Determination of the antioxidant activity of plants from Northeast Mexico. Pharm. Biol. **46**(3), 166–170 (2008)
48. Mittal, A.K., et al.: Biosynthesis of silver nanoparticles: elucidation of prospective mechanism and therapeutic potential. J. Colloid Interface Sci. **415**, 39–47 (2014)
49. Floegel, A., et al.: Comparison of ABTS/DPPH assays to measure antioxidant capacity in popular antioxidant-rich US foods. J. Food Compos. Anal. **24**(7), 1043–1048 (2011)
50. Shaji, J.; Varkey, D.: Silica-coated solid lipid nanoparticles enhance antioxidant and antiradical effects of meloxicam. J. Pharm. Investig. **43**(5), 405–416 (2013)
51. Aloqbi, A., et al.: Antioxidant activity of pomegranate juice and punicalagin. Nat. Sci. **8**(06), 235 (2016)
52. Asouri, M., et al.: Antioxidant and free radical scavenging activities of curcumin. Asian J. Chem. **25**(13), 7593–7595 (2013)
53. Untea, A., et al.: Comparison of ABTS, DPPH, phosphomolybdenum assays for estimating antioxidant activity and phenolic compounds in five different plant extracts. Bull. UASVM Anim. Sci. Biotechnol. **75**(2), 111–114 (2018)
54. Borges, A., et al.: COX inhibition profiles and molecular docking studies of the lignan hinokinin and some synthetic derivatives. Mol. Inf. **37**(12), 1800037 (2018)
55. Warner, T.D., et al.: Nonsteroid drug selectivities for cyclo-oxygenase-1 rather than cyclo-oxygenase-2 are associated with human gastrointestinal toxicity: a full in vitro analysis. Proc. Natl. Acad. Sci. **96**(13), 7563–7568 (1999)
56. Dannhardt, G.; Kiefer, W.: Cyclooxygenase inhibitors–current status and future prospects. Eur. J. Med. Chem. **36**(2), 109–126 (2001)
57. Lehmann, H., et al.: Meloxicam: a toxicology overview. Inflammopharmacology **4**(2), 105–123 (1996)
58. Matsumiya, L.C., et al.: Using the Mouse Grimace Scale to reevaluate the efficacy of postoperative analgesics in laboratory mice. J. Am. Assoc. Lab. Anim. Sci. **51**(1), 42–49 (2012)
59. Buadonpri, W., et al.: Synthetic curcumin inhibits carrageenan-induced paw edema in rats. J. Health Res. **23**(1), 11–16 (2009)
60. Tamaddonfard, E.; Farshid, A.A.; Hosseini, L.: Crocin alleviates the local paw edema induced by histamine in rats. Avicenna J. Phytomed. **2**(2), 97 (2012)
61. Osman, A.S.; Labib, D.A.; Kamel, M.M.: Carvedilol can attenuate histamine-induced paw edema and formaldehyde-induced arthritis in rats without risk of gastric irritation. Int. Immunopharmacol. **50**, 243–250 (2017)
62. Lee, S., et al.: Anti-inflammatory function of arctiin by inhibiting COX-2 expression via NF-κB pathways. J. Inflamm. **8**(1), 1–9 (2011)

63. DeWitt, D.L.: Prostaglandin endoperoxide synthase: regulation of enzyme expression. Biochim. Biophys. Acta (BBA) Lipids Lipid Metab. **1083**(2), 121–134 (1991)
64. Roy, R., et al.: Antipyretic and anti-nociceptive effects of methanol extract of leaves of Fimbristylis miliacea in mice model. J. Ethnopharmacol **243**, 112080 (2019)
65. Dhara, A., et al.: Preliminary studies on the anti-inflammatory and analgesic activity of the methanolic fraction of the root extract of Tragia involucrata Linn. J. Ethnopharmacol. **72**(1–2), 265–268 (2000)
66. Babaheydari, A.K.: In Silico drug design on aspirin for Cyclooxygenase I and II, target for reduce the effects of inflammatory. Biosci. Biotechnol. Res. Asia **12**(1), 433–444 (2015)
67. Ahmad, A., et al.: Ursolic acid rich ocimum sanctum L leaf extract loaded nanostructured lipid carriers ameliorate adjuvant induced arthritis in rats by inhibition of COX-1, COX-2, TNF-α and IL-1: pharmacological and docking studies. PLoS One **13**(3), e0193451 (2018)
68. Xu, S., et al.: Oxicams bind in a novel mode to the cyclooxygenase active site via a two-water-mediated H-bonding network. J. Biol. Chem. **289**(10), 6799–6808 (2014)
69. Blobaum, A.L.; Marnett, L.J.: Structural and functional basis of cyclooxygenase inhibition. J. Med. Chem. **50**(7), 1425–1441 (2007)
70. Kurumbail, R.G., et al.: Structural basis for selective inhibition of cyclooxygenase-2 by anti-inflammatory agents. Nature **384**(6610), 644–648 (1996)
71. Limongelli, V., et al.: Molecular basis of cyclooxygenase enzymes (COXs) selective inhibition. Proc. Natl. Acad. Sci. **107**(12), 5411–5416 (2010)
72. Regulski, M., et al.: Synthesis, in vitro and in silico evaluation of novel trans-stilbene analogues as potential COX-2 inhibitors. Bioorg. Med. Chem. **26**(1), 141–151 (2018)
73. Nguyen, H.T., et al.: Dual COX and 5-LOX inhibition by clerodane diterpenes from seeds of Polyalthia longifolia (Sonn.) Thwaites. Sci. Rep. **10**(1), 1–10 (2020)
74. Sakr, A., et al.: Design and synthesis of novel quinazolinones conjugated ibuprofen, indole acetamide, or thioacetohydrazide as selective COX-2 inhibitors: anti-inflammatory, analgesic and anticancer activities. J. Enzyme Inhib. Med. Chem. **36**(1), 1810–1828 (2021)
75. Alaa, A.M.; ElTahir, K.E.; Asiri, Y.A.: Synthesis, anti-inflammatory activity and COX-1/COX-2 inhibition of novel substituted cyclic imides. Part 1: molecular docking study. Eur J. Med. Chem. **46**(5), 1648–1655 (2011)